AIAA JOURNAL
Vol. 38, No. 8, August 2000

Modeling the Propagation of a Shock Wave Through a Glow Discharge

Jonathan Poggie*
U.S. Air Force Research Laboratory, Wright–Patterson Air Force Base, Ohio 45433-7521

Several well-known analytical solutions of the equations of gasdynamics and magnetogasdynamics were used to study the relative importance of exothermic reactions, axial temperature variation, and the magnetic field in the glow discharge tube experiments of Ganguly et al. (*Physics Letters A*, Vol. 230, 1997, pp. 218–222). In these experiments a spark was generated at one end of a tube of low-pressure argon gas, and the resulting shock pulse was allowed to propagate through a glow discharge. With the presence of the weakly ionized, nonequilibrium plasma, an acceleration and weakening of the shock pulse were observed, along with an apparent splitting of the shock. Of the three mechanisms addressed here thermal nonuniformity appears to have the most influence on the experimental results. A detonation model can probably be ruled out for two reasons. First, insufficient energy is available from electron-ion recombination reactions to drive the detonation. Second, the detonation model predicts an increase in shock density ratio with increasing heat release, in contrast to the apparent drop seen in the experiments. In a similar manner an ideal magnetohydrodynamic shock model can probably be ruled out for lack of adequate electrical conductivity and of a sufficiently strong magnetic field. This conclusion does not, however, exclude other electromagnetic phenomena, and the issue of the apparent shock splitting has not been addressed here. A combination of careful temperature measurements and numerical simulations is required to determine whether the experimental observations can be explained completely by thermal effects or physics inherent to the plasma are significant in these experiments.

Nomenclature

A, B, C	= coefficients of quadratic equation
a	= sound speed
B	= magnetic field strength
C_p	= constant pressure specific heat
C_v	= constant volume specific heat
$C^{\pm}$	= characteristic lines
e	= internal energy
H	= nondimensional heat-release parameter
h	= enthalpy
I	= current
$J^{\pm}$	= Riemann invariants $[u \pm 2a/(\gamma - 1)]$
L	= width of detonation wave system
M	= Mach number
p	= pressure
Q	= magnetic pressure parameter
q	= heat-release parameter
R	= ideal gas constant (208.13 $m^2/s^2/K$ for argon)
r	= radial distance
s	= entropy
T	= temperature
t	= time
u	= velocity
v	= specific volume
W	= shock or detonation speed
x	= position
α	= $(\gamma + 1)/(\gamma - 1)$
β	= $(\gamma - 1)/2\gamma$
γ	= adiabatic exponent (1.67 for argon)
μ_0	= permeability of free space ($4\pi \times 10^{-7}$ N/A^2)
ρ	= density
σ	= electrical conductivity

Subscripts

d	= detonation
f	= formation
I	= incident wave
R	= reflected wave
T	= transmitted wave

Introduction

EXTENSIVE experimental research has examined the effects of introducing weak, nonequilibrium ionization (fractional ionizations on the order of 10^{-8} to 10^{-6}) upstream of a shock. The speed, strength, and structure of the shock can be affected. In particular, reductions in heat transfer and drag have been claimed, based on the results of tests on wind-tunnel models. (For recent, detailed bibliographies, see, for example, Refs. 1–4.) These experimental results have revived interest in using electromagnetic effects to control the flow over hypersonic air vehicles, where conventional means of control have a substantial penalty in increased heat transfer and vehicle weight.[5]

There is, however, continuing controversy over the causes and interpretation of the phenomena observed in the experiments.[1–4] Researchers have variously attributed the changes in flow structure to a plasma-induced change in sound speed,[6] streamer structures in microwave discharges,[7] exothermic recombination reactions in the shock,[8–10] and temperature variation upstream of the shock.[11] Adamovich et al.[4] have addressed the issue of the apparent shock splitting seen in the experiments and have studied the conditions required for a steady-state, two-shock system to exist.

The present paper represents part of an ongoing study of the use of electromagnetic energy addition as a means for controlling the flow over a hypersonic vehicle. Preliminary work has addressed the implications of various mechanisms proposed to explain the experimental results. A wide variety of experiments in plasma aerodynamics have been reported, but here we will focus on a case first investigated by Klimov et al.,[12] in which a shock was generated with an electrical discharge and propagated down a tube through an ionized region.

Ganguly et al.[13] recently carried out a set of well-documented experiments on this problem. A schematic diagram of the experimental apparatus is shown in Fig. 1. The tests were carried out in

Presented as Paper 99-0867 at the AIAA 37th Aerospace Sciences Meeting, Reno, NV, 11–14 January 1999; received 1 February 1999; revision received 12 October 1999; accepted for publication 3 December 1999.

*Research Aerospace Engineer, Air Vehicles Directorate, AFRL/VAAC, 2210 Eighth Street. Senior Member AIAA.

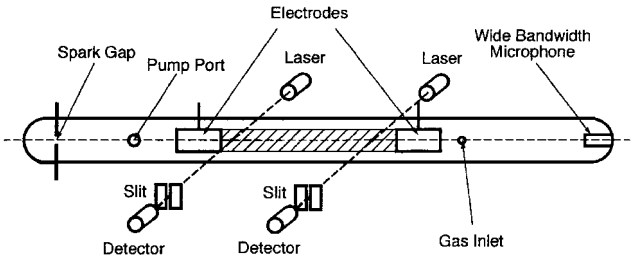

Fig. 1 Schematic diagram of experiments in glow discharge tube. (From Ganguly et al.,[13] used with permission.)

a 50-mm-diam Pyrex tube, which was roughly 1 m long and filled with argon gas. The pressure was fixed at about 4 kPa (30 torr) using a regulated purge flow. According to Hilbun,[3] the mean velocity of the purge flow was on the order of 1 m/s. A shock was generated at the spark gap (left side of diagram, 272 mm from the start of the glow discharge) with an energy release of about 100 J. Downstream of the spark gap, a pair of 30-mm-diam cylindrical electrodes, separated by 300 mm, were used to generate a longitudinal plasma, with the cathode on the left in the diagram. The discharge was operated at constant current in the range 0–140 mA, using a 10-kV, 300-mA direct current power supply.

The arrival of the shock pulse was recorded using a laser deflection technique at two stations located 302 and 422 mm from the spark gap in the positive column of the glow discharge. The lasers, slits, and photodetectors are shown schematically in Fig. 1. As the laser beam passes through the experimental apparatus, it is deflected by changes in the index of refraction brought about by density variations. The slits in front of the photodetectors cut out a portion of the deflected beam so that the amount of light reaching the photodetectors is a function of the beam deflection. The signal recorded by the photodetectors corresponds to the derivative of density along the direction normal to the slits (i.e., along the tube), averaged over the optical path.

This averaging in the transverse direction has led to a controversy about whether to accept at face value the apparent shock splitting observed by Ganguly et al. or to attribute it to an averaging of a nonuniform flow by the optical diagnostic technique.[3,4] For the present work the assumption will be made that only one shock is present in the pulse. The validity of this assumption will be examined by comparison of the calculations with the experimental data.

Calculated velocities will be compared to the average shock pulse velocity derived from measurements at two photodetector stations. The velocity of the shock pulse in the experiments is not expected to be constant over the relatively large distance between the detectors. Indeed, the pulse generated by a spark typically slows down as it expands and distributes its energy over a larger volume. The average velocity should, however, be suitable for comparison with the order-of-magnitude calculations described next.

An arrival time at each of the two photodetector stations was determined from the first rise above the ambient signal discernible by eye in the time-series plots in Ganguly et al.[13] The average velocity of the shock pulse between the two stations was determined by dividing the distance between stations (120 mm) by the difference in arrival time. The results are shown in Fig. 2 as a function of discharge current. The average velocity is seen to rise from an initial value of about 470 m/s with no current flowing to about 640 m/s at $I = 140$ mA.

An increase in shock velocity with increased current is expected because of the increase in the temperature from joule heating in the region between the two electrodes. An assessment of the nonthermal effects present in the experiments depends on how accurately the temperature field in the experiment is known. Unfortunately, temperature measurements are not available at present for the glow discharge experiments, and so a temperature calculation is necessary to quantitatively compare shock speed computations to the experiments.

To this end, Hilbun[3] carried out a steady-state, axisymmetric heat-conduction computation with a joule heating source term. He solved a nonlinear ordinary differential equation using a fourth-order Runge–Kutta shooting method to obtain the radial temperature

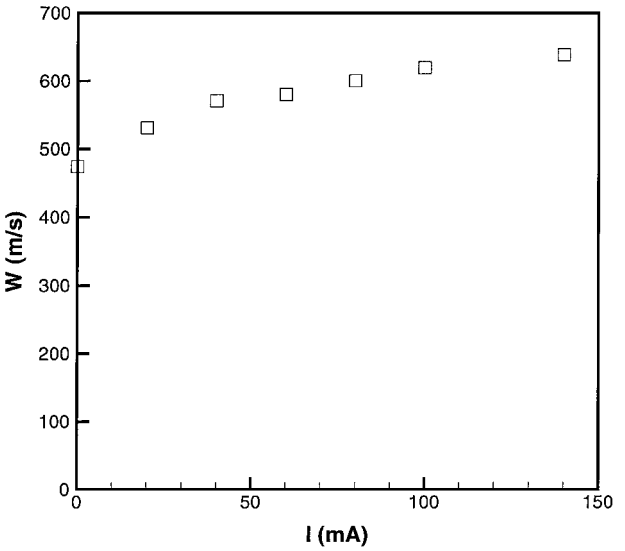

Fig. 2 Average shock pulse velocity derived from laser deflection measurements in the glow discharge tube. (Derived from the data of Ganguly et al.[13])

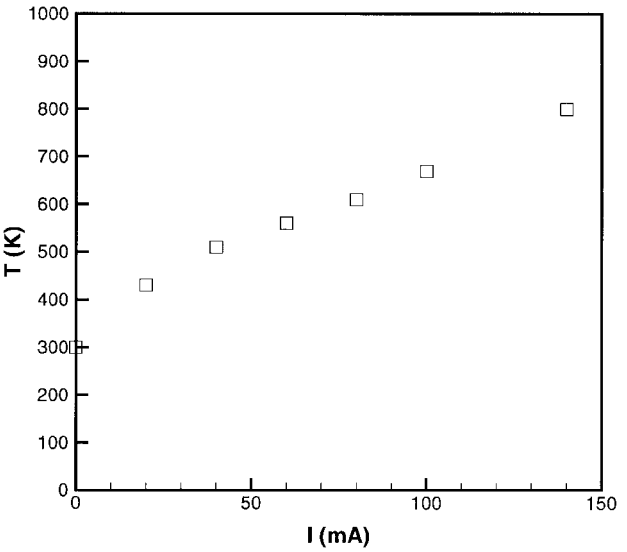

Fig. 3 Calculated temperature, averaged across the tube cross section, for the glow discharge experiments. (Data from Hilbun.[3])

profile in the region of the glow discharge and the corresponding average across the cross section. Although this model neglects (among other things) the purge flow, natural convection, and radiation, it had to be used in the calculations for lack of direct measurements.

The computed temperature, averaged across the cross section of the tube, is shown as a function of discharge current in Fig. 3. The mean temperature increases from an assumed room temperature of 300 K with current off to nearly 800 K at the maximum current of 140 mA.

The following sections will examine the relative importance of exothermic reactions, axial temperature variation, and the magnetic field in the glow discharge experiments of Ganguly et al.[13] For each of these mechanisms, an analytical model will be used to make an order-of-magnitude estimate of the conditions that would be required for that mechanism (acting alone) to explain the experimental observations. This work is intended to provide a theoretical context for discussion of the relative importance of these three effects and to identify a path for more detailed numerical simulations.

Exothermic Reactions

One proposed explanation for the effects observed in the plasma aerodynamics experiments is heat release through exothermic reactions as the gas relaxes from a nonequilibrium state.[8–10,12,14] The

basic idea is that increased species concentration downstream of the shock causes recombination reaction rates to be greatly increased, driving the state closer to equilibrium and releasing chemical energy. For this explanation to be plausible, sufficient energy must be stored in the excited gas, and adequate time must be available to release it. In the present section these issues will be addressed for the glow discharge tube experiment by using a one-dimensional analytical model to make an order-of-magnitude estimate of the required energy and time.

Here the assumption will be made that the problem of the shock propagating in a glow discharge is analogous to a shock-ignited detonation[15]: the spark generates a shock pulse that enters the ionized region, ignites an exothermic reaction, and develops into a detonation moving at constant velocity W trailed by an unsteady expansion wave. The detailed solution to this problem was apparently first considered by Taylor.[16] It is essentially a standard centered expansion fan with one uniform region replaced by the detonation wave.

Following Taylor, we solve the one-dimensional Euler equations for homentropic flow using the method of characteristics (see Thompson[17]). The form assumed for the detonation/expansion system is shown on the space-time diagram of Fig. 4. The origin corresponds to the point of ignition of the detonation. The detonation wave is indicated by a heavy line in the diagram with slope $1/W$. It compresses the initially undisturbed gas from state 1, where the velocity u is zero, to state 2, which is the beginning of the expansion. For a steady detonation the first characteristic of the expansion wave (state 2) is required to move at the detonation velocity: $u_2 + a_2 = W$. The resulting flow then expands continuously down to state 3, where the velocity must return to zero to match the boundary condition at the closed end of the tube. The expansion is a simple region[17] so that the C^+ characteristics appear in the figure as straight lines from the origin with constant slope $1/(u + a)$.

Using the fact that the C^- characteristics have the same value everywhere [$J^- = u - 2a/(\gamma - 1) = \text{const}$] and using the conditions downstream of the detonation (state 2) as a reference, we solve for the sound speed as a function of position and time:

$$\frac{a}{a_2} = 1 + \frac{\gamma - 1}{\gamma + 1}\left(\frac{x}{a_2 t} - \frac{W}{a_2}\right) \tag{1}$$

The pressure and density ratios can be found from the assumption of isentropic flow: $p/p_2 = (a/a_2)^{2\gamma/(\gamma-1)}$ and $\rho/\rho_2 = (a/a_2)^{2/(\gamma-1)}$. The velocity is given by

$$\frac{u}{a_2} = -1 + \frac{\gamma - 1}{\gamma + 1}\frac{W}{a_2} + \frac{2}{\gamma + 1}\frac{x}{a_2 t} \tag{2}$$

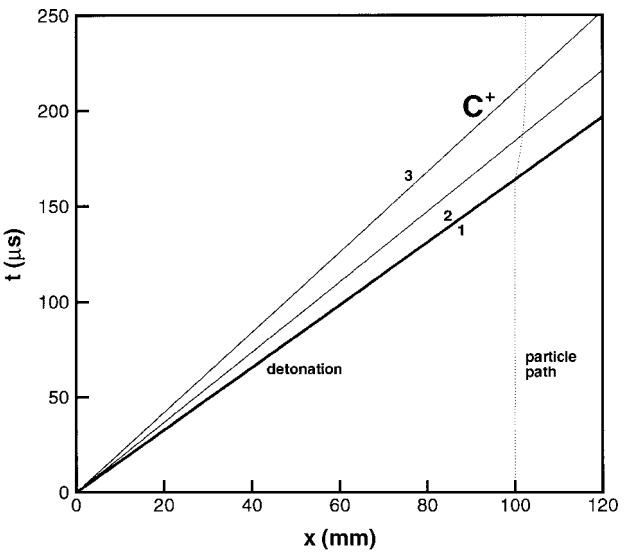

Fig. 4 Detonation/expansion system on a space-time diagram. Origin represents point where incident shock ignites detonation. Conditions: argon with $T_1 = 600$ K and $q = 20$ kJ/kg.

The jump conditions across the detonation are now needed to complete the solution.

As a simple model for the detonation, we will use the well-known approximation of an ideal-gas normal shock in which the difference in zero-point enthalpy $q = h_{f1} - h_{f2}$ is taken to be a known constant.[17–19] The adiabatic exponent γ is assumed to remain constant across the shock. With the absolute enthalpy as $h = C_p T + h_f$, the difference in enthalpy between the upstream and downstream states becomes

$$h_2 - h_1 = -q + C_p(T_2 - T_1) \tag{3}$$

The introduction of these assumptions and the ideal-gas equation of state into the usual normal shock jump conditions for mass, momentum, and energy conservation[17] leads to a Hugoniot equation of the form:

$$\frac{p_2}{p_1} = \left(2H + \frac{\gamma + 1}{\gamma - 1} - \frac{v_2}{v_1}\right)\left(\frac{\gamma + 1}{\gamma - 1}\frac{v_2}{v_1} - 1\right)^{-1} \tag{4}$$

where $H = q\rho_1/p_1$ is a nondimensional heat-release parameter. The corresponding Rayleigh line has the form

$$p_2/p_1 = 1 - \gamma M_d^2(v_2/v_1 - 1) \tag{5}$$

where $M_d = W/a_1$ is the detonation Mach number. For the present problem of a wave system propagating in a tube of reactive material, we take the the upstream thermodynamic state as specified and calculate the detonation Mach number. Assuming a Chapman–Jouget detonation, where the Rayleigh line is tangent to the Hugoniot curve, there is a unique solution to this problem. By equating the derivatives of Eqs. (4) and (5) and manipulating the results, we can find the specific volume ratio for the Chapman–Jouget detonation that occurs for a given level of heat release:

$$\frac{v_2}{v_1} = 1 + \frac{\gamma - 1}{\gamma}H - \frac{1}{\gamma}\sqrt{2\gamma\frac{\gamma - 1}{\gamma + 1}H + (\gamma - 1)^2 H^2} \tag{6}$$

This specific volume ratio can be substituted back into the Hugoniot equation (4) to obtain the corresponding pressure ratio. The detonation Mach number is

$$M_d^2 = 1 + \frac{\gamma^2 - 1}{\gamma}H + \frac{\gamma + 1}{\gamma}\sqrt{2\gamma\frac{\gamma - 1}{\gamma + 1}H + (\gamma - 1)^2 H^2} \tag{7}$$

Figure 5 shows the density profile through the detonation and expansion wave system for three values of the nondimensional heat-release parameter. The density profile can be interpreted as a snapshot of a sawtooth waveform traveling from left to right. As the wave system overtakes the undisturbed gas, a particle of fluid first

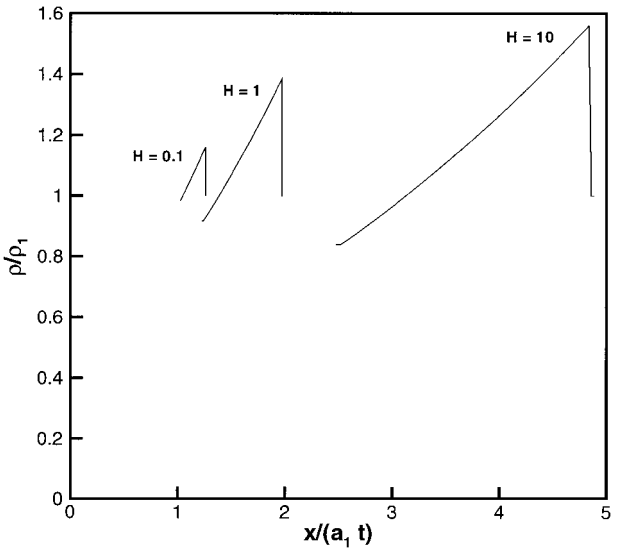

Fig. 5 Density profiles through a detonation/expansion wave system traveling in argon.

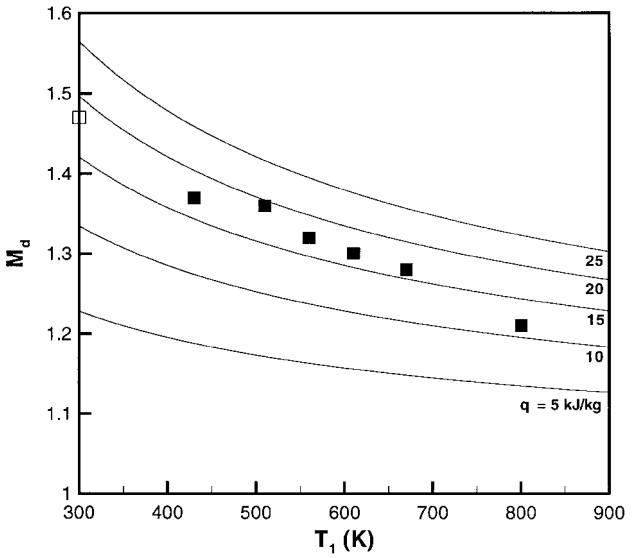

Fig. 6 Detonation Mach number as a function of upstream temperature and heat release. □, ■, average Mach number derived from the data of Ganguly et al.,[13] using the temperature calculations of Hilbun.[3]

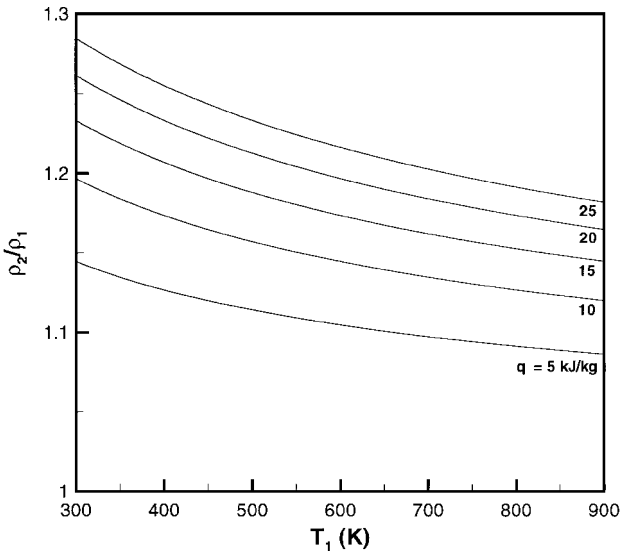

Fig. 7 Detonation density ratio as a function of temperature and heat release.

encounters the jump in density at the detonation front (right side of each waveform). From there the fluid is carried to the right until the flow expands down to zero velocity at the end of the expansion (left side of each waveform). The wave system leaves behind a region of still gas with higher pressure and lower density than the ambient conditions upstream.

With the upstream conditions held constant, the Mach number, pressure ratio, and density ratio of the detonation increase with increasing dimensional chemical energy release [Eqs. (6) and (7)]. These changes lead to the increases in the speed, width, and amplitude of the density waveform visible in the figure.

The predicted detonation Mach number from Eq. (7) is shown in Fig. 6 as function of upstream temperature for different levels of the dimensional heat-release parameter. As just noted, the detonation Mach number increases with heat release if the upstream temperature is held fixed. For a constant value of the dimensional heat release, however, the nondimensional heat-release parameter decreases with increasing temperature. Thus the detonation Mach number decreases with increasing temperature for a given level of heat release, although the dimensional velocity does increase.

The average velocities between the two photodetector stations, converted to Mach numbers according to Hilbun's predictions of the temperature averaged over the cross section, are shown as square symbols in the figure. Increasing temperature corresponds to increasing current in the experiment (see Fig. 3).

The experimental data appear to be consistent with a detonation sustained by a heat release of 15–20 kJ/kg, independent of the current. If the detonation were sustained by the energy stored in the nonequilibrium plasma, one would expect increased heat release with increased current in the glow discharge.

Further, an energy release of this order seems excessively large given the limited amount of energy that could be stored in weakly ionized argon. With an ionization energy of 38 MJ/kg (15.8 eV/atom) and a fractional ionization of 10^{-6}, less than 40 J/kg would be available to drive the detonation. For the detonation model to apply, the required energy would have to be stored in some form other than the chemical energy of ionization.

Note also the case with no plasma, indicated by a hollow symbol in the figure. No detonation will exist for this case; it represents the incident, spark-driven shock. The only requirement for this case in the present model is that the dimensional velocity of the detonation be higher than that of the incident shock so that the detonation pulse can develop. This is satisfied for the present data, but it is interesting that the zero-current case appears to lie on the same curve as the other data. The trend looks thermal.

A decrease in the amplitude of the laser deflection signal with increased discharge current was observed in the experiments. This decrease in amplitude could be caused by both a decrease in the derivative of the density along the axial direction and by the averaging of a nonuniform density field across the transverse direction.[3] If the former effect is the most significant, it indicates a decrease in shock strength with increased discharge current. The model predicts a decrease in detonation density ratio with increased temperature at fixed heat release (Fig. 7), but an increase in density ratio with increased heat release at fixed upstream temperature. As just mentioned, one would expect in the context of the detonation model that more energy would be available to drive the detonation as the discharge current was increased.

The exothermic reactions must complete rapidly for a steady detonation wave system to exist. An upper bound on the required time is the residence time of a particle in the wave system.

At a given instant in time, the wave system has a distinct width L, the distance from the detonation to the trailing edge of the expansion. The detonation travels with speed W, whereas the trailing edge travels with the local sound speed a_3. Using $u_2 = W - a_2$ and Eq. (1), it can be shown that $L = (\gamma + 1)/2\, u_2 t$.

The path of a particle starting at a position x_0 can be found by solving the equation $dx/dt = u(x, t)$, using the velocity given by Eq. (2). The solution $x(x_0, t)$ can be used to determine the time interval between when the detonation initially crosses a given fluid particle and when the particle exits the wave system. The time interval Δt is

$$\Delta t = \frac{x_0}{W}\left[\left(\frac{\gamma+1}{2} - \frac{\gamma-1}{2}\frac{W}{a_2}\right)^{-[(\gamma+1)/(\gamma-1)]} - 1\right] \quad (8)$$

As an example, consider an initial particle position of $x_0 = 100$ mm, an upstream temperature of $T_1 = 600$ K, and a heat release of $q = 20$ kJ/kg (see Fig. 4). In this case the detonation reaches the particle at about 160 μs, where the width of the sawtooth is about 20 mm and the residence time is about 50 μs. The reaction must take place within the detonation in a fraction of this time, say on the order of 10 μs or less. Otherwise, the reaction zone will be so thick that interaction with the wall boundary layer will quench the detonation.[18]

The one-dimensional model used here does not include the complex cellular structure and turbulence that are often present in detonations traveling in combustible materials. These phenomena are obviously beyond the scope of the models used in this paper, but they can be treated through numerical simulation.

Thermal Effects

This section will address the issue of thermal nonuniformity along the axial direction in the glow discharge tube experiments. The electric current flowing between the two electrodes in the experiments

generates heat (joule heating) that is carried away by conduction and convection caused by the slow purge of the working fluid. (Natural convection and radiation can also become significant for higher levels of joule heating.) These processes should produce a roughly axisymmetric temperature distribution $T(x, r)$ in the tube.

With detailed measurements of the temperature field, it should be possible to do a fairly accurate numerical simulation of the baseline thermal effects, as Hilbun[3] did with a calculated temperature distribution. Indeed, Hilbun obtained fairly good agreement with the glow discharge tube experiments in one- and two-dimensional numerical solutions of the Euler equations.[3,11] Here we will not attempt to replicate Hilbun's computations, but rather to understand the phenomena associated with thermal inhomogeneity using analytical methods. For simplicity, the thermal variations will be modeled as a contact surface located at the right of the first electrode (lumping all of the x dependence at the contact surface and averaging out the r dependence). The trailing expansion system of the spark-driven shock will be neglected. Some of the realism of the model is lost with these assumptions, but they make it possible to utilize analytical solutions. Given imprecise knowledge of the experimental conditions, the analytical solution should illustrate the basic fluid mechanics without the complexity and uncertainty of modeling the full spark-driven shock-pulse and multidimensional temperature field.

With the assumption that the only thermal nonuniformity is in the axial direction and the neglect of the trailing expansion of the spark-driven shock, the problem becomes that of a plane shock impinging at normal incidence on a plane contact surface. Early theoretical treatments of this problem were carried out by Paterson[20] and by Courant and Friedrichs.[21] A detailed experimental and theoretical study was done by Glass and Patterson[22] and Ford and Glass.[23]

The problem is illustrated in the space-time diagram of Fig. 8. The numbers designate regions of uniform flow. For $t < 0$ the incident shock propagates to the right in the diagram toward a stationary contact surface, which separates two still fluids at a given pressure (regions 1 and 5). Behind the shock lies a region (4) of uniform rightward flow at higher pressure. At $t = 0$ the shock hits the contact surface, generating transmitted and reflected waves. The transmitted wave is always a shock, but the reflected wave can be either a shock or a centered expansion fan, depending on the generalized acoustic impedance ratio of the contact surface. For the case under consideration here, where the gas on both sides of the contact surface is the same and the temperature is higher on the right, the reflected wave is an expansion. The initial and final characteristics of the expansion fan are shown in the figure, bounding a nonuniform region that separates regions 3 and 4.

Two new regions (2 and 3) appear between the reflected and transmitted waves, separated by the deflected contact surface. The pressure and velocity both match across the contact surface. The flow in these regions carries the contact surface to the right.

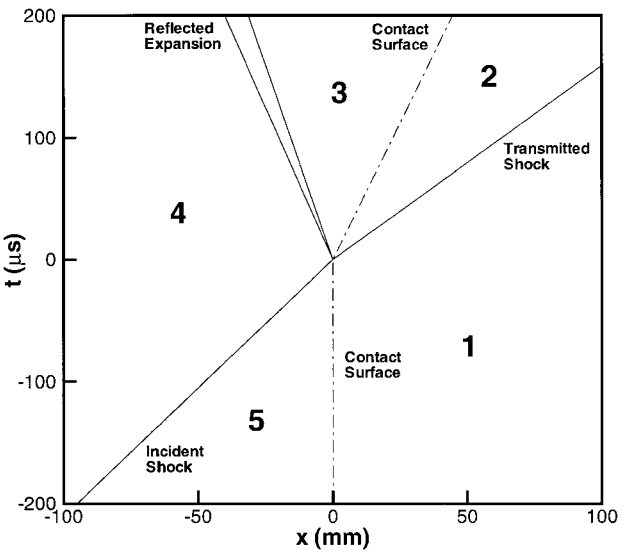

Fig. 8 Space-time diagram for normal reflection of a shock at a contact surface in argon ($M_I = 1.47$, $T_5 = 300$ K, $T_1 = 600$ K).

For the present work, we take states 1 and 5 as given, along with the strength of the incident shock. We will develop equations for the pressure as a function of particle velocity in the regions behind the reflected expansion and the transmitted shock, then match the pressure and velocity at the contact surface.

An expression for the particle velocity behind the incident shock as a function of the pressure ratio can be derived in a straightforward manner from the usual jump conditions of gasdynamics.[24] The result can be expressed as

$$\frac{u_4}{a_5} = \frac{1}{\gamma_5}\left(\frac{p_4}{p_5} - 1\right)\left(\frac{1/\beta_5}{\alpha_5 p_4/p_5 + 1}\right)^{\frac{1}{2}} \tag{9}$$

where the expressions $\alpha = (\gamma + 1)/(\gamma - 1)$ and $\beta = (\gamma - 1)/2\gamma$ have been introduced for brevity. The sound speed in region 4 is needed for calculations related to the reflected expansion fan. The ratio of sound speeds between regions 4 and 5 is given by the square root of the temperature ratio across the incident shock, which can also be found from the jump conditions.[24] The sound speed ratio is

$$\frac{a_4}{a_5} = \left(\left(\frac{p_4}{p_5}\right)\frac{\alpha_5 + p_4/p_5}{1 + \alpha_5 p_4/p_5}\right)^{\frac{1}{2}} \tag{10}$$

Because the transmitted shock also propagates into a uniform region, the expression relating the particle velocity to the pressure in region 2 is analogous to the corresponding expression for the incident shock:

$$\frac{u_2}{a_1} = \frac{1}{\gamma_1}\left(\frac{p_2}{p_1} - 1\right)\left(\frac{1/\beta_1}{\alpha_1 p_2/p_1 + 1}\right)^{\frac{1}{2}} \tag{11}$$

The solution for the reflected expansion is closely related to that discussed already for the expansion trailing a detonation wave. One important difference between the two cases is that the velocity ahead of the wave (u_4) is not zero in the present case. The expansion is a simple region, and C^+ characteristics have the value $J^+ = u + 2a/(\gamma - 1) = \text{const}$ everywhere within the wave. Using state 4 as a reference and applying the isentropic flow relation for pressure, we find the following expression relating pressure and velocity in the region behind the wave:

$$\frac{p_3}{p_4} = \left(1 + \frac{\gamma_5 - 1}{2}\left(\frac{u_4 - u_3}{a_4}\right)\right)^{1/\beta_5} \tag{12}$$

Using $p_1 = p_5$, $p_2 = p_3$, and $u_2 = u_3$, Eqs. (9–12) can be combined to give the following implicit equation for the pressure in region 3 (Refs. 22 and 23):

$$\left(\frac{p_3}{p_4} - \frac{p_5}{p_4}\right)\left(\frac{\alpha_5 + p_5/p_4}{\alpha_5 p_5/p_4 + 1}\right)^{\frac{1}{2}}\left(\frac{\beta_5 e_1/e_5}{\alpha_1 p_3/p_4 + p_5/p_4}\right)^{\frac{1}{2}} - \left(1 - \frac{p_5}{p_4}\right)\left(\frac{\beta_5}{\alpha_5 p_5/p_4 + 1}\right)^{\frac{1}{2}} + \left(\frac{p_3}{p_4}\right)^{\beta_5} - 1 = 0 \tag{13}$$

where $e = C_v T$. (An analogous expression can be obtained for the reflected shock case.[22,23]) Once the pressure p_3 is known, the speed and density ratio for the transmitted shock can be found from the usual normal shock relations.

A convenient way to display the solution is a pressure-velocity diagram, as illustrated in Fig. 9 for a contact surface in argon where $p_4/p_5 = 2.45$ ($M_I = 1.47$) and $T_1/T_5 = 2$. The known states 1 and 5 are coincident on the diagram and are indicated by a square symbol. The incident shock connects state 5 to state 4, which is also marked by a square. The curve connecting states 5 and 4 was calculated from Eq. (9) and represents all of the possible downstream states of right-running shocks with upstream state 5. In a similar fashion all of the possible transmitted shocks that originate at state 1 are computed from Eq. (11) and shown in the figure. From state 4 are shown all of the possible reflected expansions [Eq. (12)] and reflected shocks (for completeness). The solution, representing states 2 and 3, is found at the intersection of the curves for the transmitted shock and

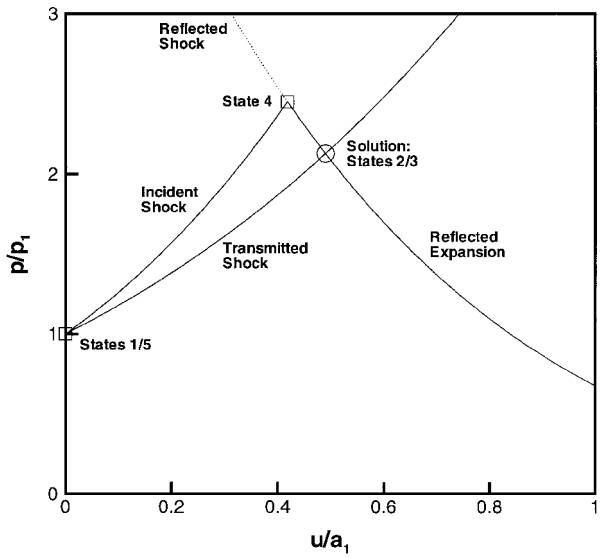

Fig. 9 Pressure-velocity diagram for normal reflection of a shock at a contact surface in argon ($M_I = 1.47$, $T_1/T_5 = 2$).

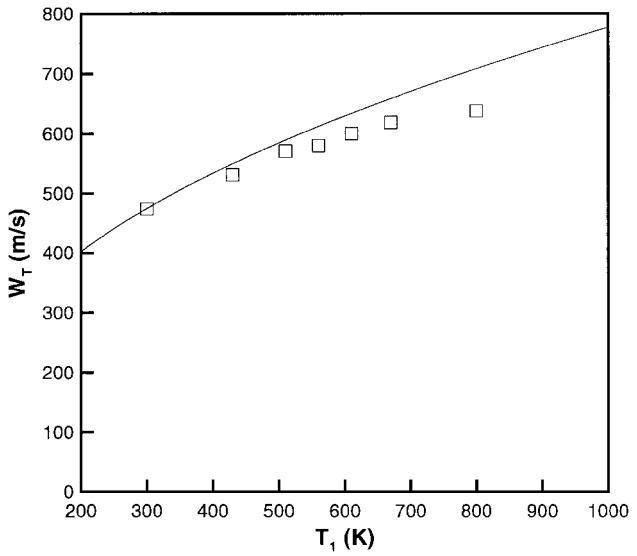

Fig. 10 Contact surface model of glow discharge experiment: ——, transmitted wave speed for $M_I = 1.47$ and $T_5 = 300$ K in argon; □, data of Ganguly et al.[13] reduced according to the calculations of Hilbun.[3]

reflected expansion. A numerical solution of Eq. (13), computed using the secant method and marked by a circle, lies at that point. The transmitted shock has a higher velocity (Fig. 8) and a lower strength (Fig. 9) than the incident shock, consistent with the observations in the glow discharge experiments.

Figure 10 shows the application of the model to the experiment, again using average velocities and the calculated temperature profile, averaged over the tube cross section.[3] The point corresponding to a temperature of 300 K represents the case with zero current in the experiment. Here there is no contact surface because there is no axial temperature variation, and so this point was used to determine the strength of the incident shock ($p_4/p_5 = 2.45$ or $M_I = 1.47$). With the incident shock specified Eq. (13) was solved numerically using the secant method for argon ($\gamma_1 = \gamma_5 = 1.67$) with $T_5 = 300$ K and varying T_1. For completeness, values of T_1 both lower (reflected shock) and higher (reflected expansion) than T_5 are shown. The predicted speed of the transmitted shock rises smoothly as the temperature in the discharge region (T_1) is increased, lying somewhat above the experimental data. Despite the simplifying assumptions made in the present analysis, the contact surface model seems to be a fair estimate of the trends seen in the experiment.

As mentioned in conjunction with Fig. 7, a decrease in the amplitude of the laser deflection signal was observed in the experiments with increased discharge current (and thus increased temperature in the discharge). This effect is consistent with the present model, as shown in Fig. 11. The predicted density ratio drops from a value just under 1.7 with no contact surface present at $T_1 = 300$ K to about 1.5 at 800 K.

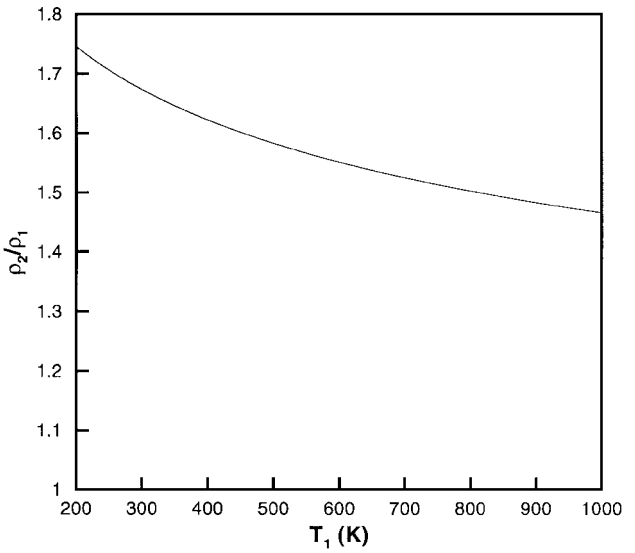

Fig. 11 Contact surface model of glow discharge experiment: ——, transmitted wave density ratio for $M_I = 1.47$ and $T_5 = 300$ K in argon.

In ongoing work thermal variations are being explored more fully through numerical solutions of the Euler equations. Combined with careful temperature measurements in the glow discharge, this approach should be able to treat accurately the baseline thermal effects present in the experiments.

Applied Magnetic Field

Purely electromagnetic effects are another possible mechanism for the results observed in the glow discharge tube experiments. Both Hilbun[3] and Adamovich et al.[4] have examined the issue of charge separation in the shock and have concluded that this mechanism has little effect on the flow for the weak ionization present in the experiments. Here we address another possibility: the effect of an applied magnetic field.

No external field was applied in the glow discharge experiments of Ganguly et al.,[13] but it is possible that the magnetic field created by the current in the glow discharge could affect the shock. An effect of a directly applied field has been observed experimentally by other research groups. For example, Gorshkov et al.[25] extended the work of Klimov et al.[12] to include an applied magnetic field and observed a reduction in shock-wave velocity when a transverse magnetic field in the range of 20–80 mT (200–800 G) was applied to a 0.4–2.7-kPa (3–20-torr) air plasma.

The additional complexity of modeling the discharge circuit and the magnetic body force makes it difficult to carry out an analysis similar to those just described for exothermic reactions and axial temperature variation. Here we will simply use the shock Mach number based on the average velocity in the experiments of Ganguly et al.[13] and estimate the order of magnitude of the strength of an upstream magnetic field that could cause a significant reduction in the density ratio across the shock.

Circumferential field lines, approximately parallel to the shock, should be set up by the current in the undisturbed discharge. We will take as a model problem a plane magnetohydrodynamic normal shock in which the magnetic field is parallel to the shock. (These assumptions restrict the possible solutions to the fast shock, excluding the slow shock and the Alfvén shock.) The electrical conductivity will be taken to be infinite (ideal magnetohydrodynamics). The jump conditions for ideal magnetohydrodynamic shocks were first derived by de Hoffmann and Teller[26] and are treated in detail in standard references on magnetohydrodynamics[27–29]

The equation of mass conservation remains the same as for an ordinary gasdynamic shock:

$$\rho_2(W - u_2) = \rho_1 W \tag{14}$$

where state 1 represents the undisturbed fluid, state 2 lies behind the shock, W is the shock speed, and u_2 is the particle speed behind the shock. The magnetic body force adds a term to the momentum equation that is equivalent to an additional effective pressure $B^2/2\mu_0$:

$$p_2 + \rho_2(W - u_2)^2 + B_2^2/(2\mu_0) = p_1 + \rho_1 W^2 + B_1^2/(2\mu_0) \quad (15)$$

Similarly, a new term $B^2/\rho\mu_0$ appears in the energy jump relation

$$h_2 + (W - u_2)^2/2 + B_2^2/(\rho_2\mu_0) = h_1 + W^2/2 + B_1^2/(\rho_1\mu_0) \quad (16)$$

An entirely new jump condition is derived from the magnetic induction equation

$$(W - u_2)B_2 = WB_1 \quad (17)$$

As for an ordinary gasdynamic shock, the velocity in the shock reference frame decreases across a magnetohydrodynamic shock so that Eq. (17) requires the magnetic field strength to increase. A corresponding current sheet must exist coincident with the shock in order to satisfy Ampère's law. The jump conditions are supplemented by the second law restriction that the entropy cannot decrease across the shock: $s_2 \geq s_1$.

Assuming an ideal ($p = \rho RT$), thermally perfect ($h = C_p T$) gas, and manipulating Eqs. (14–17), we find a quadratic equation for the density ratio across the shock:

$$A(\rho_2/\rho_1)^2 + B(\rho_2/\rho_1) + C = 0 \quad (18)$$

where

$$A = Q(2 - \gamma) \quad (19)$$

$$B = \gamma(Q + 1) + \gamma M_1^2(\gamma - 1)/2 \quad (20)$$

$$C = -\gamma M_1^2(\gamma + 1)/2 \quad (21)$$

and $Q = B_1^2/2\mu_0 p_1$ is the ratio of the effective magnetic pressure to the gas pressure on the upstream side of the shock. The shock density ratio is seen to be a function of the Mach number $M_1 = W/a_1$ and the nondimensional magnetic field strength Q.

For $\gamma < 2$, which is satisfied for ideal gases, there is one positive and one negative root of Eq. (18). Only the positive root is physically relevant.[27]

To make at least a qualitative comparison with the glow discharge tube experiments, we take argon at $p_1 = 4$ kPa and consider Mach numbers in the range observed in the experiments: $1.2 \leq M_1 \leq 1.5$. Figure 12 shows the effect of varying the upstream magnetic field strength. The required magnetic field is controlled primarily by the ambient pressure, which sets the magnitude of the nondimensional parameter Q. A significant decrease in the shock density ratio is obtained for an upstream magnetic field strength on the order of 10 mT (100 G).

This field is comparable to that imposed in the experiment of Gorshkov et al.,[25] but considerably larger than the field that would be set up by the steady current in the undisturbed discharge of the experiment by Ganguly et al. To make an order-of-magnitude estimate of the latter field, consider a current in the same range (100 mA), flowing through a straight wire: the induced field is only $B = \mu_0 I/(2\pi r) \approx 1\ \mu$T (0.01 G) at $r = 30$ mm from the wire.

One possible objection to the magnetohydrodynamic shock model is that, for relatively low values of the electrical conductivity, the magnetic Reynolds number of the flow will be low and the problem will more closely resemble a gasdynamic shock embedded in a magnetohydrodynamic channel flow. The basic parameter in question is the thickness of the magnetohydrodynamic shock relative to the dimensions of the experiment.

The problem of magnetohydrodynamic shock structure for a transverse magnetic field was solved by Marshall,[30] but an order-of-magnitude estimate of the thickness of the transition layer for the magnetic field is simply $1/(\mu_0\sigma W)$.[27] The conductivity required to obtain a thickness on the order of 10 mm with $W = 600$ m/s is on the order of $\sigma = 10^5/(\Omega \cdot \text{m})$, a rather large value. This issue needs to be reexamined with a finite-conductivity model.

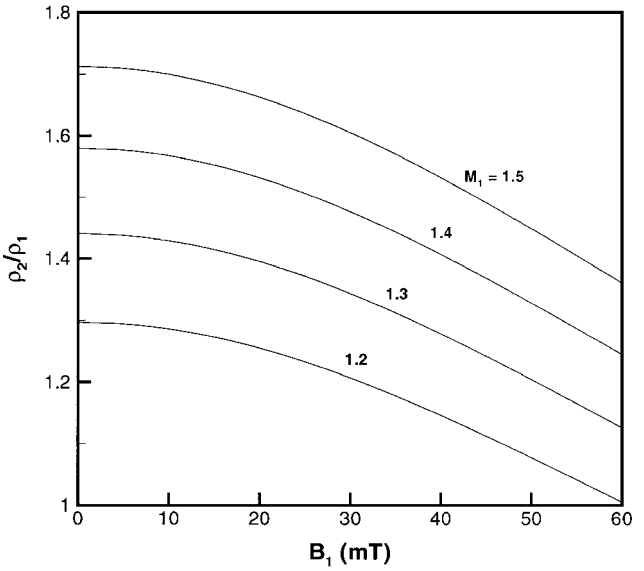

Fig. 12 Density ratio across a magnetohydrodynamic shock as a function of magnetic field strength for several different Mach numbers ($p_1 = 4$ kPa).

Conclusions

Several well-known analytical solutions of the equations of gasdynamics and magnetogasdynamics were used to study the relative importance of exothermic reactions, axial temperature variation, and the magnetic field in the glow discharge tube experiments of Ganguly et al.[13] In these experiments a spark was generated at one end of a tube of low-pressure argon gas, and the resulting shock pulse was allowed to propagate through a glow discharge. With the presence of the weakly ionized, nonequilibrium plasma, an acceleration and weakening of the shock pulse were observed, along with an apparent splitting of the shock. Of the three mechanisms addressed here, thermal nonuniformity appears to have the most influence on the experimental results. A detonation model can probably be ruled out for two reasons. First, insufficient energy is available from electron-ion recombination reactions to drive the detonation. Second, the detonation model predicts an increase in shock density ratio with increasing heat release, in contrast to the apparent drop seen in the experiments. In a similar manner an ideal magnetohydrodynamic shock model can probably be ruled out for lack of adequate electrical conductivity and of a sufficiently strong magnetic field. This conclusion does not, however, exclude other electromagnetic phenomena, and the issue of the apparent shock splitting has not been addressed here. A combination of careful temperature measurements and numerical simulations is required to determine whether the experimental observations can be explained completely by thermal effects or physics inherent to the plasma are significant in these experiments.

Acknowledgments

This project was sponsored by the U.S. Air Force Office of Scientific Research and monitored by M. Jacobs and S. Walker. This work is being carried out in collaboration with D. Gaitonde, E. Josyula, J. Schmisseur, and J. Shang. The author would like to acknowledge helpful discussions of the present work with W. Bailey, A. Creese, and R. Kimmel.

References

[1] Bain, W. L. (ed.), *Proceedings of the 1st Workshop on Weakly Ionized Gases*, 2 vols., Wright Lab. Aero Propulsion and Power Directorate, Wright–Patterson AFB, OH, 1997.

[2] Bain, W. L. (ed.), *Proceedings of the 2nd Workshop on Weakly Ionized Gases*, AIAA, Washington, DC, 1998.

[3] Hilbun, W. M., *Shock Waves in Nonequilibrium Gases and Plasmas*, Ph.D. Dissertation, Dept. of Engineering Physics, Air Force Inst. of Technology, Wright–Patterson AFB, OH, Oct. 1997.

[4] Adamovich, I. V., Subramaniam, V. V., Rich, J. W., and Macheret, S. O., "Phenomenological Analysis of Shock-Wave Propagation in Weakly Ionized Plasmas," *AIAA Journal*, Vol. 36, No. 5, 1998, pp. 816–822.

[5]Gurijanov, E. P., and Harsha, P. T., "AJAX: New Directions in Hypersonic Technology," AIAA Paper 96-4609, Nov. 1996.

[6]Mishin, G. I., "Sound and Shock Waves in a Gas Discharge Plasma," *Proceedings of the 1st Workshop on Weakly Ionized Gases*, Vol. 1, Wright Lab. Aero Propulsion and Power Directorate, Wright–Patterson AFB, OH, 1997, pp. E-1–E-12.

[7]Khodataev, K. V., "Physics of Under-Critical Microwave Discharge and Its Influence on Supersonic Aerodynamics and Shock Waves," *Proceedings of the 1st Workshop on Weakly Ionized Gases*, Vol. 1, Wright Lab. Aero Propulsion and Power Directorate, Wright–Patterson AFB, OH, 1997, pp. L-1–L-12.

[8]Bychkov, V., "Theoretical Analysis of Plasma Aerodynamic Experiments," *Proceedings of the 1st Workshop on Weakly Ionized Gases*, Vol. 1, Wright Lab. Aero Propulsion and Power Directorate, Wright–Patterson AFB, OH, 1997, pp. I-1–I-18.

[9]Kelley, J. D., "Studies of Flow Phenomena in Ionized Gases," *Proceedings of the 1st Workshop on Weakly Ionized Gases*, Vol. 1, Wright Lab. Aero Propulsion and Power Directorate, Wright–Patterson AFB, OH, 1997, pp. V-1–V-18.

[10]Zaslonko, I. S., "Non-Equilibrium Kinetic Effects in Shock Waves," *Proceedings of the 1st Workshop on Weakly Ionized Gases*, Vol. 1, Wright Lab. Aero Propulsion and Power Directorate, Wright–Patterson AFB, OH, 1997, pp. N-1–N-52.

[11]Bailey, W. F., and Hilbun, W. M., "Baseline of Thermal Effects on Shock Propagation in Glow Discharges," *Proceedings of the 1st Workshop on Weakly Ionized Gases*, Vol. 2, Wright Lab. Aero Propulsion and Power Directorate, Wright–Patterson AFB, OH, 1997, pp. GG-1–GG-18.

[12]Klimov, A. I., Koblov, A. N., Mishin, G. I., Serov, Y. L., and Yavor, I. P., "Shock Wave Propagation in a Glow Discharge," *Soviet Technical Physics Letters*, Vol. 8, No. 4, 1982, pp. 192–194.

[13]Ganguly, B. N., Bletzinger, P., and Garscadden, A., "Shock Wave Damping and Dispersion in Nonequilibrium Low Pressure Argon Plasmas," *Physics Letters A*, Vol. 230, 1997, pp. 218–222.

[14]Vstovskii, G. V., and Kozlov, G. I., "Propagation of Weak Shock Waves in a Vibrationally Excited Gas," *Soviet Physics: Technical Physics*, Vol. 31, No. 8, 1986, pp. 911–914.

[15]Gaydon, A. G., and Hurle, I. R., *The Shock Tube in High-Temperature Chemical Physics*, Reinhold, New York, 1963.

[16]Taylor, G. I., "The Dynamics of the Combustion Products Behind Plane and Spherical Detonation Fronts in Explosives," *Proceedings of the Royal Society of London A*, Vol. 200, 1950, pp. 235–247.

[17]Thompson, P. A., *Compressible-Fluid Dynamics*, McGraw–Hill, New York, 1972; self-published, 1988.

[18]Williams, F. A., *Combustion Theory: The Fundamental Theory of Chemically Reacting Flow Systems*, 2nd ed., Addison–Wesley, Redwood City, CA, 1985.

[19]Landau, L. D., and Lifshitz, E. M., *Fluid Mechanics*, 2nd ed., Pergamon, Oxford, 1987.

[20]Paterson, S., "The Reflection of a Plane Shock Wave at a Gaseous Interface," *Proceedings of the Physical Society*, Vol. 61, No. 2, 1948, pp. 119–121.

[21]Courant, R., and Friedrichs, K. O., *Supersonic Flow and Shock Waves*, Interscience, New York, 1948.

[22]Glass, I. I., and Patterson, G. N., "A Theoretical and Experimental Study of Shock-Tube Flows," *Journal of the Aeronautical Sciences*, Vol. 22, No. 2, 1955, pp. 73–100.

[23]Ford, C. A., and Glass, I. I., "An Experimental Study of One-Dimensional Shock-Wave Refraction," *Journal of the Aeronautical Sciences*, Vol. 23, No. 2, 1956, pp. 189–191.

[24]Anderson, J. D., *Modern Compressible Flow, with Historical Perspective*, McGraw–Hill, New York, 1982.

[25]Gorshkov, V. A., Klimov, A. I., Koblov, A. N., Mishin, G. I., Khodataev, K. V., and Yavor, I. P., "Propagation of Shock Waves in a Glow Discharge Plasma in the Presence of a Magnetic Field," *Soviet Physics: Technical Physics*, Vol. 29, No. 5, 1984, pp. 595–597.

[26]de Hoffmann, F., and Teller, E., "Magneto-Hydrodynamic Shocks," *Physical Review*, Vol. 80, No. 4, 1950, pp. 692–703.

[27]Ferraro, V. C. A., and Plumpton, C., *An Introduction to Magneto-Fluid Mechanics*, Oxford Univ. Press, Oxford, 1961.

[28]Sutton, G. W., and Sherman, A., *Engineering Magnetohydrodynamics*, McGraw–Hill, New York, 1965.

[29]Jeffrey, A., *Magnetohydrodynamics*, Interscience, New York, 1966.

[30]Marshall, W., "The Structure of Magneto-Hydrodynamic Shockwaves," *Proceedings of the Royal Society of London A*, Vol. 233, 1955, pp. 367–376.

M. Sichel
Associate Editor